NOAA Technical Report NESS 79

Error Characteristics of Satellite-Derived Winds

Washington, D.C.
June 1979

U.S. DEPARTMENT OF COMMERCE
National Oceanic and Atmospheric Administration
National Environmental Satellite Service

NOAA TECHNICAL REPORTS

National Environmental Satellite Service Series

...tal Satellite Service (NESS) is responsible for the establishment and operation ...llite systems of NOAA.

... in NOAA Technical Report NESS series will not preclude later publication in an ... in scientific journals. NESS series of NOAA Technical Reports is a continua... the consecutive numbering sequence of, the former series, ESSA Technical Report ...tellite Center (NESC), and of the earlier series, Weather Bureau Meteorological ...Satellite Laboratory (MSL) Report. Reports 1 through 39 are listed in publication NESC 56 of this series.

Reports in the series are available from the National Technical Information Service (NTIS), U.S. Department of Commerce, Sills Bldg., 5285 Port Royal Road, Springfield, VA 22161, in paper copy or microfiche form. Order by accession number, when given, in parentheses. Beginning with 64, printed copies of the reports, if available, can be ordered through the Superintendent of Documents, U.S. Government Printing Office, Washington, DC 20402. Prices given on request from the Superintendent of Documents or NTIS.

ESSA Technical Reports

NESC 44 Processing and Display Experiments Using Digitized ATS-1 Spin Scan Camera Data. M. B. Whitney, R. C. Doolittle, and B. Goddard, April 1968, 60 pp. (PB-178-424)

NESC 45 The Nature of Intermediate-Scale Cloud Spirals. Linwood F. Whitney, Jr., and Leroy D. Herman, May 1968, 69 pp. plus appendixes A and B. (AD-673-681)

NESC 46 Monthly and Seasonal Mean Global Charts of Brightness From ESSA 3 and ESSA 5 Digitized Pictures, February 1967-February 1968. V. Ray Taylor and Jay S. Winston, November 1968, 9 pp. plus 17 charts. (PB-180-717)

NESC 47 A Polynomial Representation of Carbon Dioxide and Water Vapor Transmission. William L. Smith, February 1969 (reprinted April 1971), 20 pp. (PB-183-296)

NESC 48 Statistical Estimation of the Atmosphere's Geopotential Height Distribution From Satellite Radiation Measurements. William L. Smith, February 1969, 29 pp. (PB-183-297)

NESC 49 Synoptic/Dynamic Diagnosis of a Developing Low-Level Cyclone and Its Satellite-Viewed Cloud Patterns. Harold J. Brodrick and E. Paul McClain, May 1969, 26 pp. (PB-184-612)

NESC 50 Estimating Maximum Wind Speed of Tropical Storms From High Resolution Infrared Data. L. F. Hubert, A. Timchalk, and S. Fritz, May 1969, 33 pp. (PB-184-611)

NESC 51 Application of Meteorological Satellite Data in Analysis and Forecasting. Ralph K. Anderson, Jerome P. Ashman, Fred Bittner, Golden R. Farr, Edward W. Ferguson, Vincent J. Oliver, Arthur H. Smith, James F. W. Purdom, and Rance W. Skidmore, March 1974 (reprint and revision of NESC 51, September 1969, and inclusion of Supplement, November 1971, and Supplement 2, March 1973), pp. 1--6C-18 plus references.

NESC 52 Data Reduction Processes for Spinning Flat-Plate Satellite-Borne Radiometers. Torrence H. MacDonald, July 1970, 37 pp. (COM-71-00132)

NESC 53 Archiving and Climatological Applications of Meteorological Satellite Data. John A. Leese, Arthur L. Booth, and Frederick A. Godshall, July 1970, pp. 1-1--5-8 plus references and appendixes A through D. (COM-71-00076)

NESC 54 Estimating Cloud Amount and Height From Satellite Infrared Radiation Data. P. Krishna Rao, July 1970, 11 pp. (PB-194-685)

NESC 56 Time-Longitude Sections of Tropical Cloudiness (December 1966-November 1967). J. M. Wallace, July 1970, 37 pp. (COM-71-00131)

NESS 55 The Use of Satellite-Observed Cloud Patterns in Northern Hemisphere 500-mb Numerical Analysis. Roland E. Nagle and Christopher M. Hayden, April 1971, 25 pp. plus appendixes A, B, and C. (COM-73-50262)

(Continued on inside back cover)

NOAA Technical Report NESS 79

Error Characteristics of Satellite-Derived Winds

Lester F. Hubert and
Albert Thomasell, Jr.

Washington, D.C.
June 1979

U.S. DEPARTMENT OF COMMERCE
Juanita M. Kreps, Secretary

National Oceanic and Atmospheric Administration
Richard A. Frank, Administrator

National Environmental Satellite Service
David S. Johnson, Director

CONTENTS

Abstract - 1

1. Introduction - 1

2. Comparison of satellite winds and rawins - - - - - - - - - - - - 3

2.1 NESS Picture pair winds for a winter period - - - - - - - - 3

2.1.1. Data and statistics - - - - - - - - - - - - - - - - - - 3

2.1.2. Vector difference summaries - - - - - - - - - - - - - - 4

2.1.3. Fixed versus variable height of picture pair winds - - 4

2.2 NESS picture pair winds for a summer period - - - - - - - - 7

2.3 NESS upper level winds for a summer period - - - - - - - - 8

2.4 Estimation of error in NESS operational wind data - - - - 9

3. Errors in cloud tracking (system noise) - - - - - - - - - - - - 13

3.1 Self-comparison error estimates of low level cloud motion vectors - 13

3.2 Errors in low cloud vectors calculated from tracking experiments - 22

3.2.1. Description of the experiments - - - - - - - - - - - - 22

3.2.2. Estimates of error under optimal conditions - - - - - - 25

3.2.3. Error incurred by reduced resolution - - - - - - - - - 27

3.2.4. Errors added by decreased time interval - - - - - - - - 28

3.3 Errors in low cloud vectors calculated from simultaneous measurements - - - - - - - - - - - - - - - - - 30

3.3.1. Data and method of analysis - - - - - - - - - - - - - - 30

3.3.2. Results - 31

3.4 Summary of errors in cloud tracking (system noise) - - - 32

4. Summary and conclusions - 33

References - 34

TABLES

2.1 Root mean square of vector magnitude differences of analyzed wind fields as function of horizontal distance and elevation, m s^{-1} - - 10

2.2--Vector magnitude difference between satellite winds and rawins at level assigned to satellite wind and mean satellite wind speed, m s^{-1} - 12

2.3--Estimates of vector magnitude error for satellite winds - - - - - 12

3.1--Measured departure values D for operational picture pair vectors on a 2.5° grid, m s^{-1} - 19

3.2--Measured departure values D_d for September 1974 GATE winds, m s^{-1} - 20

3.3--Estimates of the random observational errors of NESS low level cloud motion vectors - 21

3.4--Differences between low cloud tracks derived by various methods over a 90-minute interval, degrees, m s^{-1} - - - - - - - - 24

3.5--Differences between cloud motions measured over three successive 30-minute intervals, degrees, m s^{-1} - - - - - - - - - - - - - - - - 26

3.6--Increase of "noise" in computer-tracked vectors associated with halving the time interval, degrees, m s^{-1} - - - - - - - - - - - 29

3.7--Vectors magnitude differences between co-located simultaneous cloud vectors, m s^{-1} - 31

FIGURES

2.1--Cumulative frequencies vs. magnitude of vector difference between Azores rawin at various levels and nearby NESS low level cloud vectors for Nov. 1976 through Feb. 1977. Inset: Frequency distribution of pressure (height) of the level of least difference (LBF) between satellite and station wind observation - - - - - - - - - - - 5

2.2--Same as 2.1, for Bermuda - 5

2.3--Same as 2.1, for Guadalupe Island - - - - - - - - - - - - - - - - - 5

2.4--Same as 2.1, for Midway Island - - - - - - - - - - - - - - - - - - - 5

2.5--Same as 2.1, for Sable Island - - - - - - - - - - - - - - - - - - - 6

2.6--Same as 2.1, for Ship C-7-H and miscellaneous ships - - - - - - - 6

2.7--Same as 2.1, for combination of all island and ship data - - - - 6

2.8--Cumulative frequencies vs. magnitude of vector difference between 900-mb rawin and nearby low cloud vectors. Bermuda Guadalupe, Midway, Sable and ships encompassed in the envelope curve--Azores the single curve - - - - - - - - - - - - - - 6

2.9--Cumulative frequencies vs. magnitude of vector difference between 900-mb rawin and nearby low level NESS low cloud vectors for July and August 1978 - - - - - - - - - - - - - - - - - 8

2.10--Cumulative frequencies vs. magnitude of vector difference between rawins and nearby NESS upper level cloud vectors at various heights, for July and August 1978 - - - - - - - - - - - - 8

3.1--Typical NESS picture pair vectors for the northeast Pacific, 0900 GMT July 1, 1978 - 14

3.2--Picture pair vectors selected from the set of 3.1 at central points of 5^{o} blocks that have vectors at three or four corners. A full barb represents 10 kt - 15

3.3--Average vectors calculated for each of the central points shown on figure 3.2 - 15

3.4--Average vectors of figure 3.3 (long barbs) plotted over the original central vectors of figure 3.2 (short barbs). Locations with single vectors show the original corner vectors used in the averaging process - 16

3.5--The basic 5^{o} grid block used for vector error calculations (2.5^{o} grid) - 17

3.6--A typical set of dense cloud motion vectors from the GATE wind set, 1500 GMT, September 3, 1974 - - - - - - - - - - - - - - - - - 20

3.7--Visible picture for 12:30 GMT, September 15, 1974, showing area used in the AOIPS tracking experiment - - - - - - - - - - - - - - - 23

3.8--Coordinate system used with the AOIPS tracking experiment to measure along-track and cross-track and directional difference - 25

ERROR CHARACTERISTICS OF SATELLITE-DERIVED WINDS

by

Lester F. Hubert and Albert Thomasell, Jr.
Meteorological Satellite Laboratory
National Environmental Satellite Service, NOAA
Washington, D.C.

ABSTRACT. Errors of winds derived from geostationary satellite measurements are estimated by analysis of differences between satellite and rawin observations. It is estimated that the NESS winds contain root mean square errors (rmse) of 4.7 m s^{-1} for low levels and 8.5 m s^{-1} for upper levels. These errors stem from the "noise" inherent in measuring cloud displacements and errors introduced by meteorological influences. "System noise," evaluated by three independent techniques, amounts to rms vector magnitudes of 2.5 to 3.0 m s^{-1} for picture pair vectors and about 4 m s^{-1} for manual vectors. These figures pertain only to clouds tracked with infrared imagery.

The accuracy of these data can be increased by reducing system noise, but improving their meteorological value can be realized only by modifying procedures to enable clouds to be tracked in meteorologically active regions.

1. INTRODUCTION

This report presents estimates of errors in wind observations derived from geostationary satellite data, based on analysis of differences between satellite winds and nearby rawinsondes and examines in some detail the error component of satellite winds we call "system noise." Wind errors are made up of two parts a) errors arising from the variable relation between cloud motion and wind (at a specified level), and b) errors inherent in tracking clouds with satellite imagery. The latter is a pervasive "system noise" while the former depends upon atmospheric conditions which can introduce errors that range from insignificant to major. Perhaps the greatest atmospheric effect is that associated with vertical wind shear. Shear may introduce a motion component of its own to convective clouds. Even in the absence of such nonadvective motion, vertical shear produces serious wind errors when cloud-drift vectors are assigned to wrong elevations.

Present data are inadequate for appraising atmospheric effects, but we can assess the "system noise" and thereby gain some insight into the error characteristics of satellite winds.

Accuracy estimates of winds perch uneasily on the weak twig of "ground truth." Except for a few measurements made during field experiments

(Hasler et al. 1976 and 1977) the "truth" itself is fraught with uncertainty. Moreover, these independent observations of wind are commonly somewhat removed in space and time from satellite measurements. Space-time variations of the wind, together with the random errors in measuring the "true" wind fields, contribute to the differences between satellite winds and independent data.

Earlier studies such as Bauer (1976) and Hubert and Whitney (1974) conclude that satellite winds were about as accurate as were rawins. This conclusion bears closer scrutiny and some amplification--one of the tasks undertaken here.

Rawinsonde accuracy decreases when the balloon, rising into layers of great speed, moves a great distance from the station. Error is thereby correlated with both speed and altitude and it has been expressed in terms of root mean square error (rmse) as a percentage of speed. For example see Arnold (1956) and Gabriel and Bellucci (1951). Such a relation is not appropriate to satellite observations because large cloud displacement (high speed) usually is associated with smaller percentage error.

Satellite errors stem from other sources. For example, the relation is unknown between the motion of clouds some kilometers thick and wind which is changing with altitude. In the lower troposphere cumuli are the most common target and their motion relative to a shearing flow is particularly complex (Hubert 1976). Thus, when displacements of cumuli are reported as winds at a specific elevation, this complexity can introduce errors that range from smaller to much larger than those of rawinsondes.

When the problems associated with convective clouds can be avoided by tracking thin clouds, another error source appears in its place--that of determining cloud temperature (and thereby altitude). This is especially troublesome with cirrus.

Because the error sources are different, no fixed relation exists between satellite and rawin errors. Moreover, the satellite wind errors due to atmospheric conditions are likely to be influenced by a different set of atmospheric variables in the low troposphere than in the middle and upper atmosphere. Hence, studies of low cloud motions in a limited variety of synoptic situations are probably not representative of all satellite winds. For these reasons, earlier studies which found "about the same accuracy" of rawin and satellite data, need some amplification.

The next section presents summaries of the deviation between satellite and rawinsonde observations. By estimating the different factors that enter into the differences between these data sets, we isolate the error of satellite winds. Also examined is the effect of letting low cloud motions represent the wind at the 900-mb level. Section 3 reports three independent assessments of cloud tracking accuracy (system noise); section 4 summarizes the studies of error characteristics and points out features of a wind derivation system that can be improved to increase the accuracy of the present operational product.

2. COMPARISON OF SATELLITE WINDS AND RAWINS

Nearly all the NESS operational winds for low levels are derived automatically from pairs of infrared images taken at 30-minute intervals. They are transmitted world-wide as 900 mb wind observations[1], and their accuracy is assessed by comparing them with rawin reports at that level. Upper clouds, tracked manually on movie loops, are assigned to a variety of pressure levels, and comparisons with rawins are made for the pressure level assigned to the satellite winds.

2.1 NESS Picture Pair Winds for a Winter Period

Summaries presented in this section pertain to vector magnitude differences between cloud motions over water and nearby balloon measurements from ships and island stations. Separation between clouds and rawin stations ranged from 100 km to 350 km and they differed in time by two hours. Upper air data from coastal stations were not used because we found that their observations were not always representative of the wind that existed some 300 km seaward where the clouds were tracked.

2.1.1 Data and Statistics

Picture pair winds for the months November 1976 through February 1977 were paired with rawins for 0000 GMT and 1200 GMT from the following stations:

Station No. and Name	No. of Comparisons[2]	Summarized on figure no.
08509 Azores	163	2.1
78016 Bermuda	184	2.2
76151 Guadalupe	109	2.3
91066 Midway	299	2.4
72600 Sable	226	2.5
C-7-H Ship:38°N.71°W	163	2.6
miscellaneous ships	42	
Total - - - - - -	1186	

[1]The practice of assigning all low level data to 900 mb was the result of an earlier study that showed the average agreement with rawins was slightly better at 900 mb than at any other single pressure level. This is confirmed by this study.

[2]In some cases two satellite observations were paired with a single rawin observation, thereby providing a greater number of comparisons than the number of rawin observations during the period.

Deviations between cloud drift vectors and rawin observations were tabulated for 1000 mb, 900 mb, 800 mb and 700 mb and for the level of best fit (LBF). The LBF is defined as the level at which the vector difference between rawin and cloud motion is smallest. Deviations in terms of vector magnitude differences, as well as LBF pressures to the nearest centibar, were summarized separately for each station, with the exception of the ship data which were combined as noted above.

A LBF was not found for every comparison. In some cases differences between rawin and cloud vector were identical at two or more elevations. These cases were discarded. In addition some cases were classified as "No LBF" where the minimum difference exceeded the rawin wind speed. Cloud vectors falling into this "No LBF" category, about 5% of the total sample, were divided into two groups -- those with cloud speeds exceeding 5 m s^{-1} and those with lesser speeds. The latter correspond to data which, while uncertain, would not seriously degrade a synoptic scale analysis because usually the rawin speeds were also small. Those cloud speeds exceeding 5 m s^{-1}, on the other hand must be counted as significantly different from balloon data and are included in the statistics. All cloud motions, including those in the "No LBF" category, were also compared to rawins at the constant pressure levels.

2.1.2 Vector Difference Summaries

Figures 2.1 to 2.6 show cumulative percent frequencies versus vector magnitude differences. Figure 2.7 combines the data from figures 2.2 to 2.6. Only the 900-mb curves are shown as solid lines--other levels are depicted by unconnected symbols. Insets to these figures show the frequency distributions of the LBF pressures in 5 cb class intervals, as well as the frequency of "No LBF" where the speed exceeded 5 m s^{-1}.

Steep slope of a cumulative frequency curve indicates good agreement between cloud drift and balloon vectors. For example the 900-mb curve of figure 2.7, rising sharply and remaining to the left of the curves for other levels, shows that the correspondence to 900-mb rawins is closer than at any other fixed level. By reason of its definition, the LBF curve must always lie to the left of other points. Note that the percent deviations at LBF do not accumulate to 100% because of the "No LBF" category.

It is clear that the Azores data are significantly different from the others. Figure 2.8 shows the Azores 900-mb curve together with the envelope of all other 900-mb curves. The histograms of LBF pressures suggest the reasons for this difference. For most of the stations (fig. 2.7) modes occur at high pressures and the median LBF is near 900 mb. Azores LBF pressures, by contrast, (fig. 2.1) show that a significant proportion of the cloud drift winds correspond to the 650- to 750-mb balloon measurements.

2.1.3 Fixed versus Variable Height of Picture Pair Winds

The foregoing shows that assigning picture pair vectors to the 900-mb level

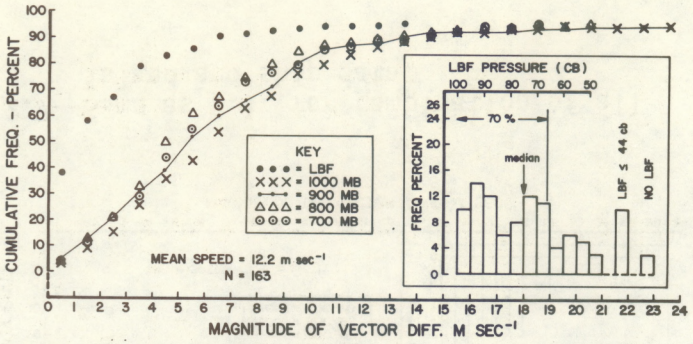

Figure 2.1--Cumulative frequencies vs. magnitude of vector difference between Azores rawin at various levels and nearby NESS low level cloud vectors for Nov. 1976 through Feb. 1977. Inset: Frequency distribution of pressure (height) of the level of least difference (LBF) between satellite and station wind observation.

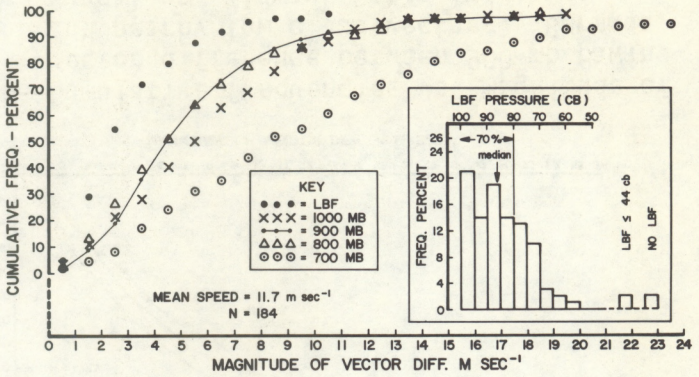

Figure 2.2--Same as 2.1, for Bermuda.

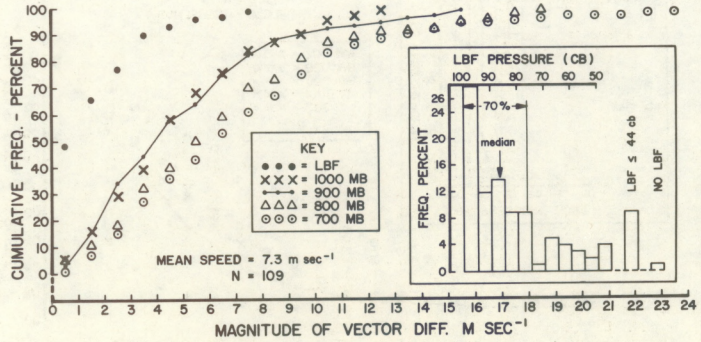

Figure 2.3--Same as 2.1, for Guadalupe Island.

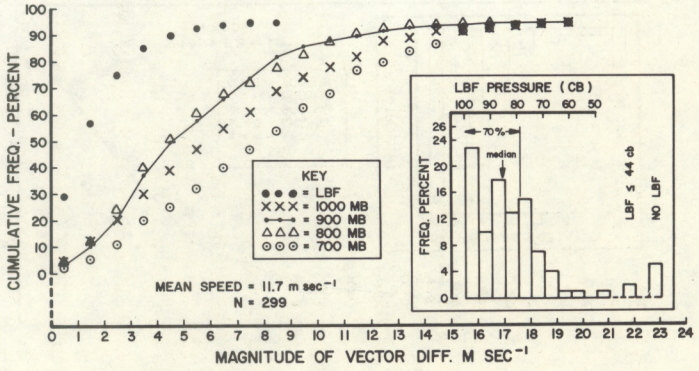

Figure 2.4--Same as 2.1, for Midway Island.

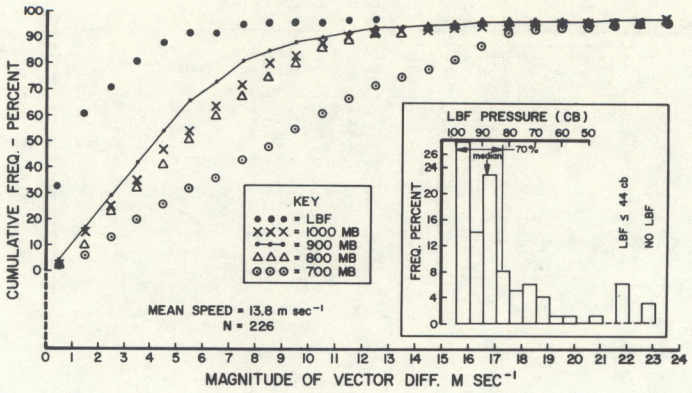

Figure 2.5--Same as 2.1 for Sable Island.

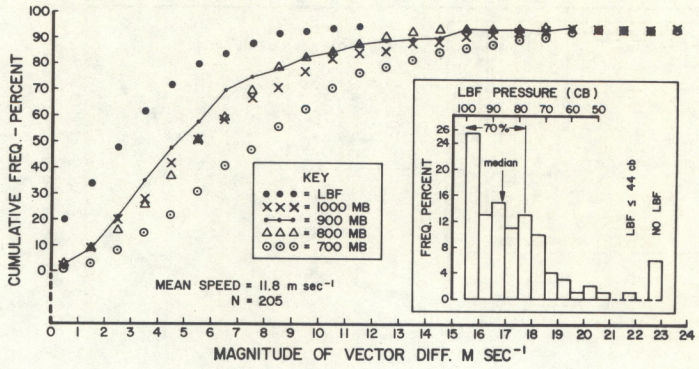

Figure 2.6--Same as 2.1, for Ship C-7-H and miscellaneous ships.

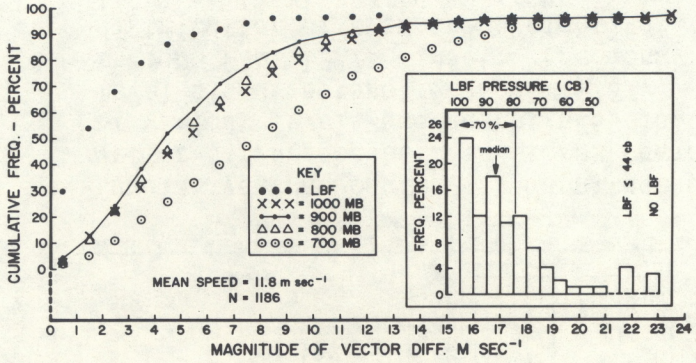

Figure 2.7--Same as 2.1, for combination of all island and ship data.

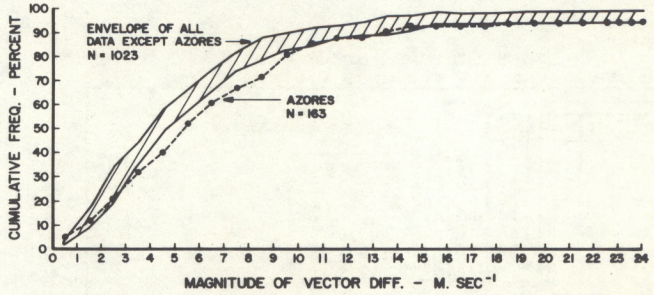

Figure 2.8--Cumulative frequencies vs. magnitude of vector difference between 900-mb rawin and nearby low cloud vectors. Bermuda, Guadalupe, Midway, Sable and ships encompassed in the envelope curve--Azores the single curve.

or to any other fixed pressure level, introduces error. The contrast between Azores and all other data appears to be real. At least for that location, picture pair winds in winter might better be assigned to 800 mb. This no doubt stems from a meteorological effect but its nature is unknown. It may simply be that the frequency of altocumuli in the 650 to 750 mb layer is greater here than at other locations. We have no ready means of investigating this possibility. Analysis of cloud top temperatures would not settle the question because low clouds whose motions correspond to the 900-mb wind frequently extend to 650 or 750 mb.

Several years ago in a joint MSL--Office of Operations project we experimented with assigning height to low cloud vectors on the basis of cloud temperature. Differences between cloud motions and rawins at those variable heights exceeded the differences at 900 mb--a result consistent with our earlier conclusion that cumuli pattern motions correspond to wind near cloud base.

A more recent experiment sought to relate the level of best fit to the synoptic situation by associating LBF with wind direction and 850 mb temperature. This also failed to reduce the difference between rawins and picture pair vectors.

Several researchers at the University of Wisconsin and at Goddard Space Flight Center (personal communications) have assigned low cloud vectors to a variety of heights--mostly on the basis of adjusted cloud top temperatures. Their goal was to obtain low-level wind analyses for purposes other than to compare satellite winds with rawins. Accordingly none of these authors studied the effect of variable height assignments or showed them to be superior to fixed-level assignments.

We must conclude that at the present state of the art, no technique has a demonstrated capability for improving the assignment of height to picture pair vectors over water. However, this conclusion may not be valid for other situations and other tracking methods--for example, manually tracking small cumuli over land. Neither does it foreclose the possibility of assigning heights to variable elevation of cloud bases according to climatology. Note that this conclusion applies only to picture pair winds derived from infrared images.

2.2 NESS Picture Pair Winds for a Summer Period

Deviations between 900-mb rawins and picture pair measurements for 7 weeks during July and August 1978 were obtained with a program different from that used for the winter period. Differences at levels other than 900 mb were not calculated nor were LBF pressures obtained. Coastal station data, eliminated from the earlier period, were included. The separation criteria were also altered. South of 30° latitude, observations were paired if the separation did not exceed 2° latitude and 2° longitude. Poleward of 30° the separation distances did not exceed 2° latitude and 3° longitude. This permits maximum separation of 360 km near 30°. We have no record of the mean separation distance in this data set, but believe it to be about the

same as the winter set where the mean separation was 290 km. These changes may have introduced additional deviations, compared to the winter deviations, but they are used here to increase the sample size. They are the output of a program set up for an international comparison of satellite winds and we did not feel the time and expense of a duplicate run, with the earlier program, was justified. Figure 2.9 displays vector magnitude cumulative frequencies of picture pair data for these summer data.

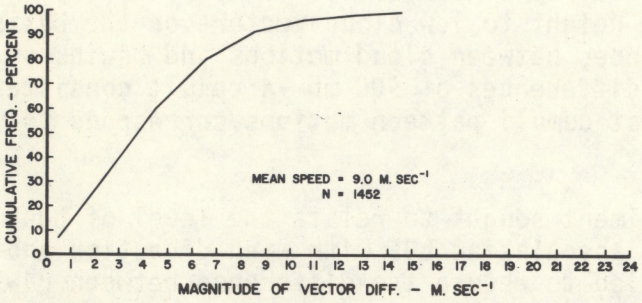

Figure 2.9--Cumulative frequencies vs. magnitude of vector difference between 900-mb rawin and nearby low level NESS low cloud vectors for July and August 1978.

2.3 NESS Upper Level Winds for a Summer Period

Upper level winds measured with movie loops and assigned to a variety of levels above the 700 mb pressure level during this summer period were compared with rawins at the assigned levels. Separation criteria were identical to those for the summer picture pair data. Figure 2.10 is a plot of vector magnitude frequencies, similar to the earlier figures.

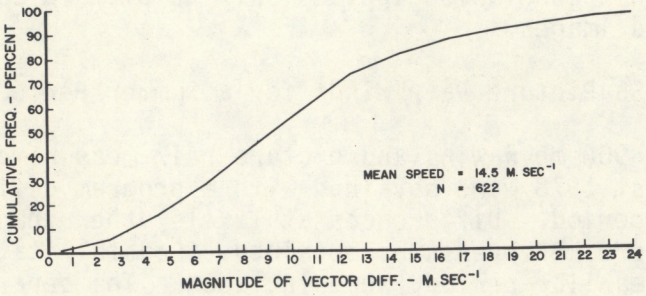

Figure 2.10--Cumulative frequencies vs. magnitude of vector difference between rawins and nearby NESS upper level cloud vectors at various heights, for July and August 1978.

2.4 Estimates of Error in NESS Operational Wind Data

Differences between rawins and satellite winds such as those summarized in figures 2.3 to 2.10 are the sum of several components. In this section, by means of some reasonable assumptions, we estimate the part of those differences that is due to errors in satellite winds.

Consider the vector magnitude difference (Z) between a rawin at point a and a satellite wind at point b for N cases:

$$Z^2 = \Sigma(R_a - S_b)^2/N \qquad (2.1)$$

and $R_a = W_a + e_r$

$S_b = W_b + e_s$, where

R_a : rawin measurement of wind at a specific level, at point a, time t_1

S_b : satellite measurement of wind at a specific level, at point b, time t_2

W_a : true (error-free) synoptic scale wind at point a, t_1.

W_b : true synoptic scale wind at point b, t_2

ΔW : $(W_a - W_b)$--Time-space difference of the true synoptic scale flow.

e_r : random error of rawin measurement,

e_s : random error of satellite measurement of wind,

Substituting

$$Z^2 = \Sigma[\Delta W + (e_r - e_s)]^2/N$$

$$= [\Sigma\Delta W^2 + \Sigma e_r^2 + \Sigma e_s^2 + 2\Sigma\Delta W(e_r - e_s) - 2\Sigma e_r e_s]/N \qquad (2.2)$$

The last two terms can be dropped because they are each the summed product of random variables which vanish for large N. Approximately, therefore,

$$Z^2 = \frac{\Sigma\Delta W^2}{N} + \frac{\Sigma e_r^2}{N} + \frac{\Sigma e_s^2}{N}. \qquad (2.3)$$

The quantity ΔW represents the time-space difference of the error-free, synoptic scale wind at points a and b. The two error terms, e_r and e_s, represent the differences between that actual large (synoptic) scale wind and those respective measurements. These errors stem from different causes. Rawin error, e_r, consists of measurement errors plus differences between the synoptic scale wind and the turbulent wind that advects the balloon. The latter might be regarded as a scale error. Satellite wind error, e_s, consists of cloud tracking errors and all differences that exist between cloud motion and the synoptic scale wind at the assigned height. Scale error is assumed to be negligibly small because cloud motions correspond to large scale flow. Upper clouds, for example, are tracked for 2 hours over distances in excess of 100 km. Picture pair vectors (low clouds) correspond to large scale flow because they are derived from the displacement of cloud ensembles that occupy squares about 125 km on a side.

Cloud tracking errors, which are but one component of satellite error, are examined in the next section. Here we are concerned with estimating the total rms error of satellite winds, namely, $[(\Sigma e_s^2)/N]^{1/2}$. We will evaluate that error using measured values of Z, estimates of ΔW made from independent statistics, and with some assumptions regarding the relative magnitudes of e_r and e_s.

Operational NMC analyses of winds were used to estimate the quantity $(\Sigma \Delta W^2)/N$, as follows. For a given time and pressure level, the differences of the u-component of wind (Δu) and the v-component of wind (Δv) were computed successively over distances of 1, 2, 3, 4, and 5 grid distances from about 8° to 55° north latitude. Weighted for map scale in this zone, the mean grid spacing is 291 km. The rms of each different component was summarized and combined to yield the rms of the vector magnitude difference. That is,

$$\text{rms (vector difference)} = \left\{ \left[\text{rms } (\Delta u)\right]^2 + \left[\text{rms } (\Delta v)\right]^2 \right\}^{1/2}$$

These were calculated for three pressure surfaces and are listed in table 2.1.

Table 2.1 Root mean square of vector magnitude differences of analyzed wind fields as function of horizontal distance and elevation, m s^{-1}

	Distance Km				
	291	582	873	1164	1455
Pressure-ht					
850 mb	2.9	5.2	6.9	8.1	9.1
500 mb	4.6	8.6	11.7	14.0	15.8
(300 mb)*	(6.4)	(12.0)	(16.4)	(19.7)	(22.1)
250 mb	7.1	13.3	18.1	21.7	24.3

*Interpolated linearly on a log-pressure scale.

Because satellite winds were derived from images only 2 hours from the rawin observation times, time changes are neglected, therefore,

$$\text{rms (vector diff)} \simeq [(\Sigma\Delta W^2)/N]^{1/2}$$

The calculated values increase with height linearly with log of pressure at all distances and this relation was used to interpolate rms values for the 300-mb level which is representative of the upper level winds.

Using rms (vector difference) as an estimate of $[(\Sigma\Delta W^2)/N)]^{1/2}$ in eq. (2.3) makes the implicit assumption that spatial variability of the real synoptic scale wind is depicted by the NMC analyses. This appears to be valid because we do not depend on the analysis to represent the actual wind at every grid point; rather, we imply only that the analyses exhibit the same statistical characteristics as the real wind. That is, the scale and amplitude of disturbances of the real and analyzed fields are assumed to be identical.

Satellite wind errors contain a component due to height assignment that is essentially absent from rawin measurements. That is, (eq. 2.3) $\Sigma e_s^2 > \Sigma e_r^2$ and for the purpose of partitioning error between these two terms, we assume that their ratio lies in the range from 3/2 to 2/1. That is, $\Sigma e_r^2 = R\Sigma e_s^2$ where R lies in the range from 0.67 to 0.50.[3] Substituting in eq. (2.3) and rearranging,

$$\Sigma e_s^2/N = [Z^2-(\Sigma\Delta W^2)/N]/(1+R). \qquad (2.4)$$

We now have estimates of all the terms on the right hand side of this equation and can compute the probable range of rms errors in satellite winds. These errors represent the rms differences between the satellite wind (reported as the wind at a specific level) and the real synoptic scale wind at that level. Table 2.2 contains the values of Z, and from table 2.1 we take the estimates of $\Sigma\Delta W^2/N$ for the 850-mb and the 300-mb levels to compute the picture pair and the upper level wind errors, respectively. The average distance between satellite wind and upper air station was about 290 km so the two table 2.1 values to be used are 2.9 m s^{-1} and 6.4 m s^{-1}. The assumed values $0.67 \geqslant R \geqslant 0.50$ yield the range of error estimates listed in table 2.3.

---

[3]The exact value of this ratio is unknown, but the ultimate result is not very sensitive to the value used, as long as R<1. Ratios less than unity obtain when satellite wind error is greater than rawin error. The evidence presented here, as well as the consensus of those involved in deriving satellite winds, is that the uncertainty in assigning heights to cloud motions vectors creates a strong tendency for R<1.

Table 2.2 Vector magnitude difference between satellite winds and rawins at level assigned to satellite wind and mean satellite wind speed, m s^{-1}

Date Sample	N	Median	rms	Mean wind speed
Picture pair: all island and ship data for winter 1977	1186	4.3	6.98	11.8
All island and ship data except Azores	1023	4.1	6.74	11.7
Azores	163	5.3	8.30	12.2
Picture pair: summer 1978	1452	3.7	6.30	9.0
All picture pair data for winter 1977 and summer 1978 - weighted mean	2638	4.0	6.61	10.2
Manual (upper level) winds, summer 1978	622	9.2	12.40	14.5

Table 2.3 Estimates of vector magnitude error for satellite winds

Data sample	Range* of rms m s^{-1}
Picture pair: all island and ship data for winter 1977	From 4.9 to 5.2
All island and ship data except Azores	" 4.7 to 5.0
Azores	" 6.1 to 6.3
Picture pair: summer 1978	" 4.3 to 4.6
All picture pair data for winter 1977 and summer 1978, weighted mean	" 4.6 to 4.8
Manual (upper level) winds, summer 1978	" 8.2 to 8.7

*See text for explanation of these upper and lower limits

The result is insensitive to the assumed value for R as illustrated by the following: Table 2.3 shows the total sample of picture pair winds to have an rms error ranging from 4.6 to 4.8 m s^{-1}. If we assume that the satellite error is three times greater than the rawin error, so that R = 0.33, this upper limit of 4.8 is changed to 5.2 m s^{-1}. If we assume that the satellite error were equal to the rawin error, the lower limit becomes 4.2 m s^{-1}.

In summary, this analysis shows the rmse (vector magnitude) of satellite winds probably lies in the ranges:

Picture pair 900-mb winds: rmse 4.6 to 4.8 m s^{-1}

Upper level winds : rmse 8.2 to 8.7 m s^{-1}

The contrast between errors for upper level and lower level winds shows that the random errors of satellite winds cannot be adequately expressed by a single figure nor, as discussed earlier, be expressed as a function of wind speed.

The error figures just cited may be overestimates. They derive from the assumption that all the differences between balloon and cloud drift measurements are due to two independent, random errors. This may not always be true. In addition, the presence of a few extreme errors in each set of satellite winds tends to exaggerate the rms deviations from rawins. Figure 2.10, for example, shows that 5% of the differences exceeded 21 m s^{-1}. In many situations these extreme errors would be easily detected by the wind field analysis procedure. Perhaps the error might be reflected more accurately by the smallest 95% of the deviations. Moreover, it should be emphasized that the errors in table 2.3 pertain to individual vectors and that no account has been taken of the density of satellite winds relative to rawins. The ultimate objective, accurate analysis of the wind field, is enhanced by great data density. These factors should be considered carefully by users of satellite wind observations in order fully to exploit the meteorological information in these data.

3. ERRORS IN CLOUD TRACKING (SYSTEM NOISE)

The previous section treated error pertaining to measuring the wind with satellite data and pointed out that these errors are the sum two separate components. One of these is the error inherent in measuring cloud motions which we call "system noise." This section evaluates that component by three independent methods; self-comparison, tracking experiments, and simultaneous vectors. Results are comparable and lend greater credibility than would be deserved by any one method.

3.1 Self-comparison Error Estimates of Low Level Cloud Motion Vectors

This method of estimating cloud tracking error was devised initially for picture pair vectors which are calculated by NESS three times daily on a regular grid extending over wide areas. With slight modification it is also

applicable to dense networks of irregularly spaced vectors. Here it is applied to the GATE Wind Sets (Martin et al. 1975, Chatters et al. 1977). This latter application is especially useful for estimating error characteristics which can then be used to further analyze picture pair errors. A typical set of picture pair vectors is shown in figure 3.1. Where cloud targets permit, winds on the regular grid network are available at each corner of a 5^0 square, with an additional wind at the center of the square.

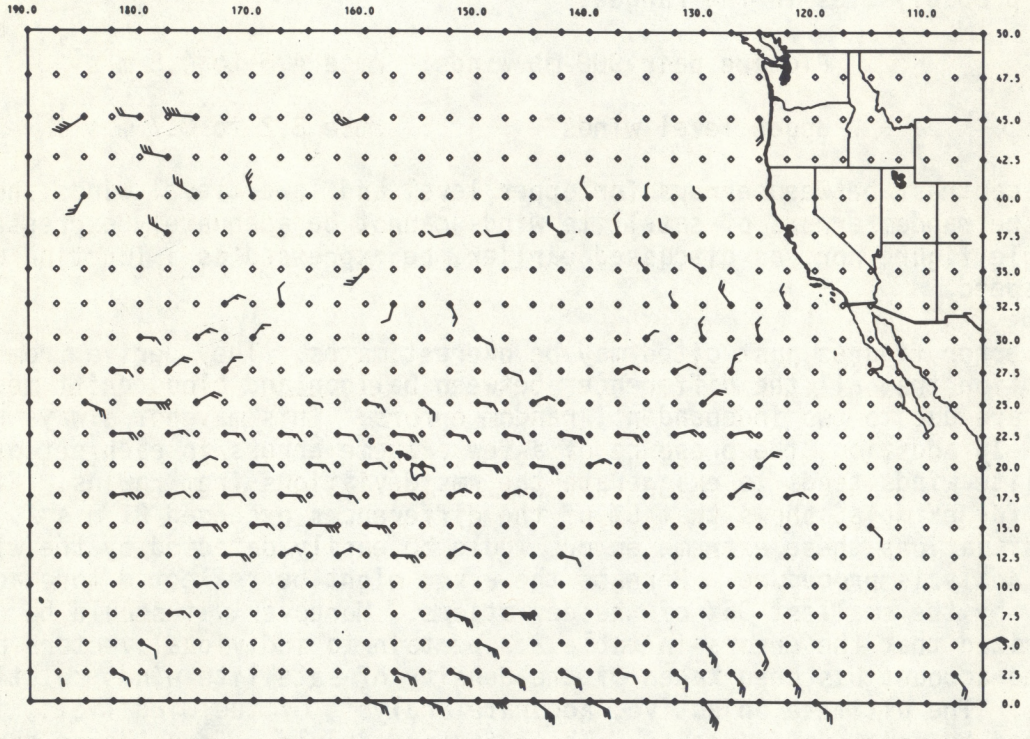

Figure 3.1--Typical NESS picture pair vectors for the northeast Pacific, 0900 GMT July 1, 1978.

The method calculates an error estimate for one set of winds at a time (the set in figure 3.1 for example), then those estimates are grouped and averaged for some meaningful period.

The first step in calculating an error estimate is to identify those winds that are centrally located in a 5^0 square, where at least 3 of the 4 corners of the square have a wind. Figure 3.2 illustrates these central winds for the wind set of figure 3.1. Next, the vector average of the winds at the 3 or 4 corners is calculated and is assigned to the central point of the square (see fig. 3.3). The departure of the original wind at the central point from the colocated average wind is computed for all such central points and provides the basic measurement for the error estimates. These departures are shown graphically in figure 3.4 at the gridpoints where two vectors are plotted.

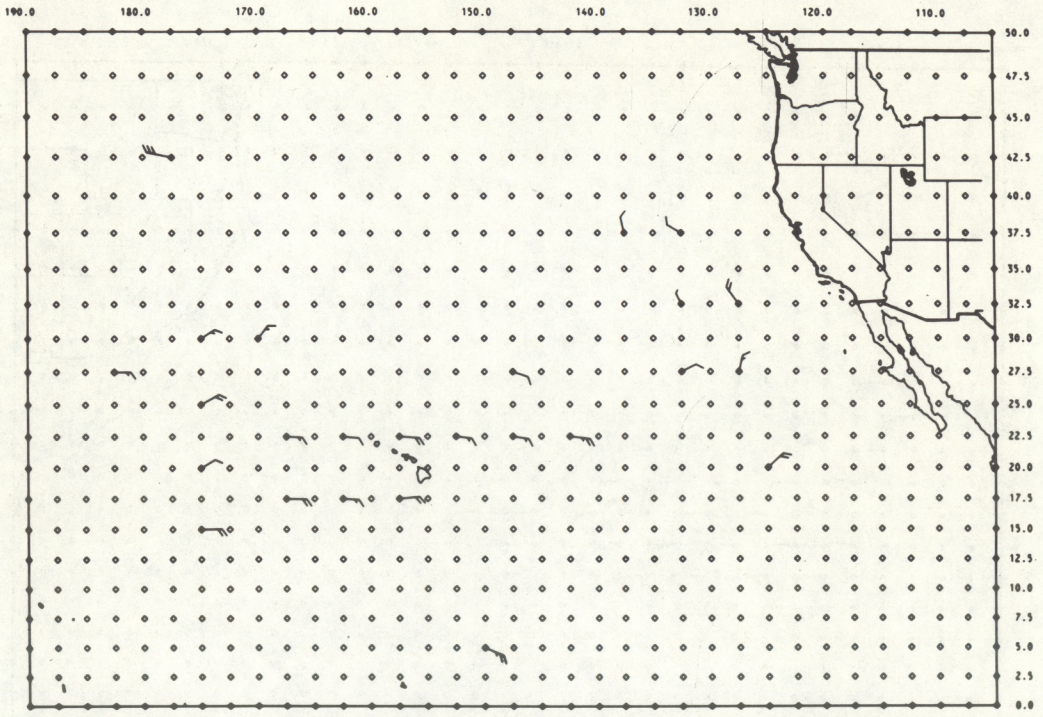

Figure 3.2--Picture pair vectors selected from the set of 3.1 at central points of 5° blocks that have vectors at three or four corners. A full barb represents 10 kt.

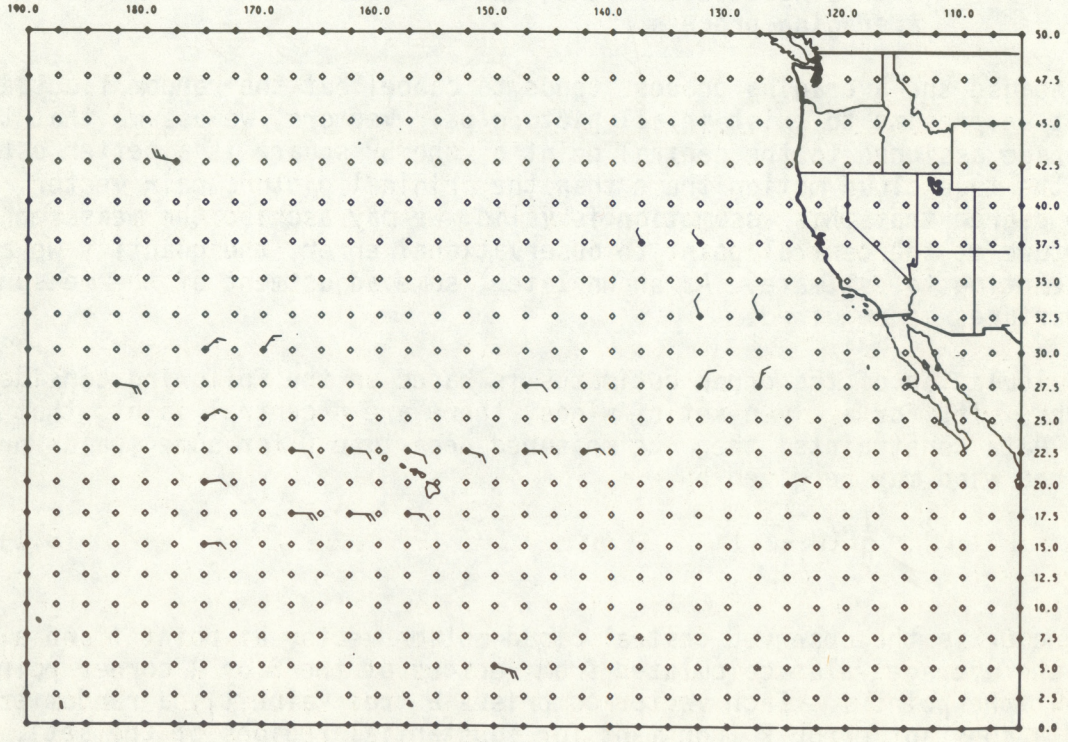

Figure 3.3--Average vectors calculated for each of the central points shown on figure 3.2.

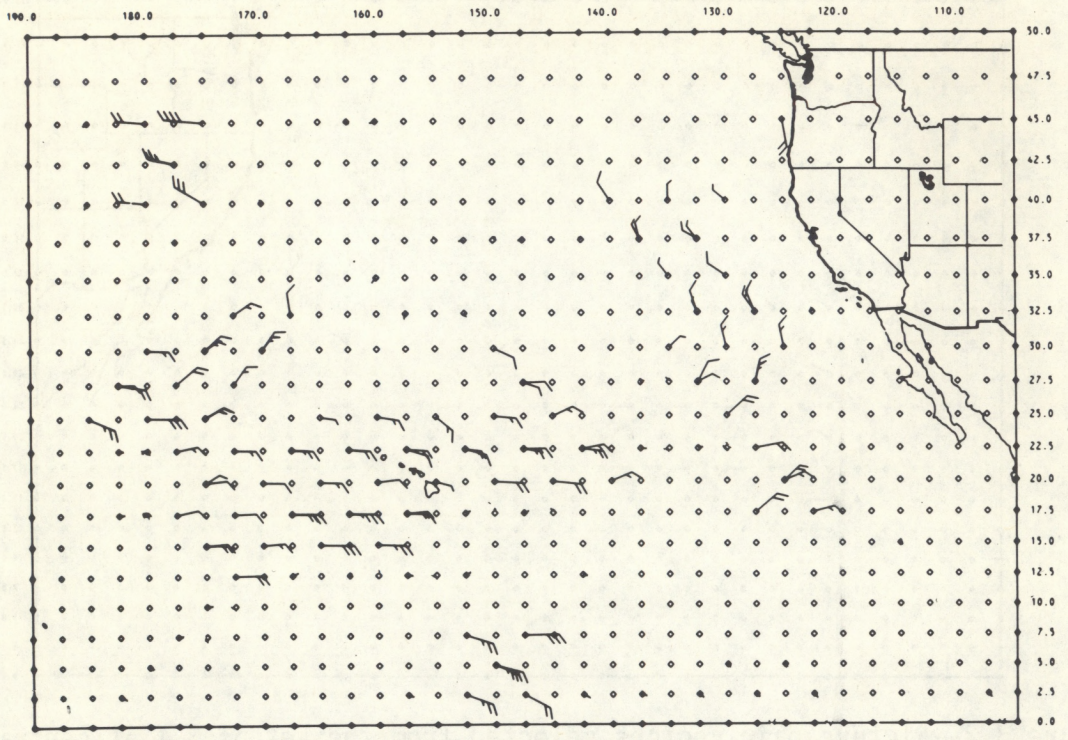

Figure 3.4--Average vectors of figure 3.3 (long barbs) plotted over the original central vectors of figure 3.2 (short barbs). Locations with single vectors show the original corner vectors used in the averaging process.

Because the averaging process tends to cancel out the random fluctuations that we presume to exist in all picture pair vectors, we assume that the average assigned to the central point of the 5^{o} square is a better estimate of the true cloud motion there than the original picture pair vector. To the degree that this assumption is valid, we may ascribe the measured departure at the central point to observational error, the quantity we are attempting to estimate. As shown later, some adjustment of the measured departures is required.

Calculation of the error estimates is based on the following considerations. If, for a given set of winds, there are n central points that satisfy the data constraints, then the measured departure D for some scalar property of the wind may be given by

$$D^2 = \frac{1}{n}\Sigma(O_i-\bar{a}_i)^2 \qquad (3.1)$$

where O_i is the observed central cloud motion vector at point i and $\bar{a}_i$ is the average value calculated from vectors at the 3 or 4 corner points about the point i. Each vector comprises a true value t_i, a random error e_i, and a constant error k (constant for substantial regions of the set).

Figure 3.5 shows the basic 5^0 block used in the computations, the 4 corner points where at least 3 vectors are required, and the central point i. This will be referred to as a gridmesh of 2.5^0.

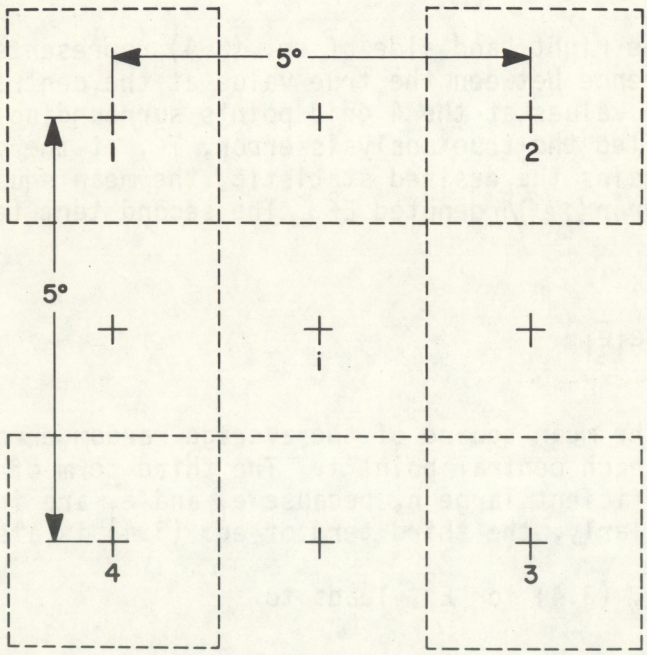

Figure 3.5--The basic 5^0 grid block used for vector error calculations (2.5^0 grid).

The average value calculated for the central point i is given by

$$\bar{a}_i = \frac{1}{m}\Sigma(t_{im}+e_{im}+k) = \bar{t}_i+\bar{e}_i+k \qquad (3.2)$$

where m represents the points 1 through 4 in figure 3.5, t_{im} is the true value at each point m, and e_{im} is the random error at point m. For picture pair vectors the maximum m is 4, one located at each of the 4 corners. For dense nonregular data, it is possible that each point will have a cluster of vectors about it. In this case many measurements will determine the averages. With a large sample, the sample mean of a random variable such a e_i in eq. (3.2) will be close to zero. In the case of picture pair vectors where the maximum sample size is 4, it is improbable that the sample mean of e_i will be zero. For this reason $\bar{e}_i$ is retained as a yet-to-be determined variable in eq. (3.2) and elsewhere.

If in eq. (3.1) we replace O_i with $t_i + e_i + k$ and $\bar{a}_i$ with eq. (3.2), we get

$$D^2 = \frac{1}{n}\Sigma(t_i+e_i+k-\bar{t}_i-\bar{e}_i-k)^2 \qquad (3.3)$$

The systematic error, k drops out and eq. (3.3) expands to

$$D^2 = \frac{1}{n}\Sigma(t_i-\bar{t}_i)^2+ \frac{1}{n}\Sigma(e_i-\bar{e}_i)^2+ \frac{2}{n}\Sigma(t_i-\bar{t}_i)(\bar{e}_i-e_i) \qquad (3.4)$$

The first term on the right hand side of eq. (3.4) represents the mean square of the difference between the true value at the central points i and the mean of the true values at the 4 grid points surrounding each point i. This quantity is called the true analysis error, T^2, at the central points. The second term contains the desired statistic, the mean square of the random observational error $(\Sigma e_i^2)/n$ denoted E^2. The second term (eq. 3.4) expands into the expression

$$E^2 + \bar{E}^2 - \frac{2}{n}\Sigma e_i \bar{e}_i$$

where $\bar{E}^2 = (\Sigma \bar{e}_i^2)/n$, the mean square of the average random error of observations available for each central point i. The third term of this expression becomes zero for sufficient large n, because e_i and $\bar{e}_i$ are independent random variables. Similarly, the third term of eq. (3.4) is also zero.

The solution of eq. (3.4) for E^2, leads to

$$E^2=D^2-T^2-\bar{E}^2. \qquad (3.5)$$

Of the three terms on the right hand side of eq. (3.5), only D^2 is measured directly. Both T and $\bar{E}$ must be estimated by other means to obtain a value for E. The analysis error T represents the departure of the true cloud motion at the central point i from the true block average and it will approach zero as the grid mesh on which it is computed becomes very small. The term $\bar{E}$ depends on the number of observations that entered into the determination of each individual $\bar{e}_i$; the greater the number of observations, the more likely that $\bar{E}$ will be small.

For a dense network of observations processed on a small enough gridmesh, we may assume that T and $\bar{E}$ are negligible and that

$$E_d^2 = {}^*D_d^2, \qquad (3.6)$$

where the subscript denotes dense data and the asterisk a fine gridmesh. The value of E given by eq. (3.6) does not depend upon data density or grid distance; it does depend upon the data sets and the procedure used for calculating winds. Thus if the picture pair procedure produced sufficiently dense vector sets we could select a fine grid mesh and calculate directly the picture pair cloud motion error E. Unfortunately, picture pair calculations are made on a 2.5^o grid, which is judged to be too coarse to allow either T or $\bar{E}$ to be ignored.

The analysis error T depends on grid mesh and on the variability in the true motion field but it does not depend upon the procedure that produces winds. Therefore we may use a dense data network, process the data with a grid mesh that matches the picture pair gridmesh (2.5°), and calculate a value of T that is applicable to picture pair vectors. With dense data, $\overline{E}^2$ may be neglected and eq. (3.5) may be rewritten

$$T^2 = D_d^2 - E_d^2. \tag{3.7}$$

Further eq. (3.6) may be substituted for E_d^2 to give

$$T^2 = D_d^2 - *D_d^2, \tag{3.8}$$

where T^2 is valid for the same gridmesh used in calculating D_d^2. A typical set of dense data, extracted from the GATE wind set, is shown in figure 3.6.

Tables 3.1 and 3.2 present the basic measurements used to estimate observational errors. Departure measurements, D, for NESS operational

Table 3.1 Measured departure values D for operational picture pair vectors on a 2.5° grid, m s^{-1}

	New VISSR data base				Old data base		
	rms	rms	rms		rms	rms	rms
Date	u	v	$\lvert\delta\vec{V}\rvert$	Date	u	v	$\lvert\delta\vec{V}\rvert$
Jan. 78	2.6	2.2.	3.4	Jan. 77	2.5	1.9	3.1
Dec. 77	2.5	2.3	3.4	Dec. 76	2.5	2.0	3.1
Nov. 77	2.1	2.3	3.1	Nov. 76	2.4	1.9	3.1
Mean	2.4	2.3	3.3		2.5	1.9	3.1

picture pair vectors on a 2.5° grid mesh are given in table 3.1; the parameters are the u and v vector components and the absolute magnitude of the vector difference. Table 3.2 contains measurements D_d for similar parameters, but for the dense network in the GATE wind set. Where table 3.1 gives data only for the 2.5° grid mesh, table 3.2 gives data for a range of grid meshes extending from 1° to 3°.

Table 3.2 Measured departure values D_d for September 1974 GATE winds, m s^{-1}

Grid mesh	rms u	rms v	rms $\lvert\delta\vec{V}\rvert$
1^o	1.5	1.5	2.1
1.5^o	1.7	1.5	2.3
2.0^o	1.9	1.6	2.5
2.5^o	1.9	1.6	2.5
3.0^o	2.1	1.9	2.9

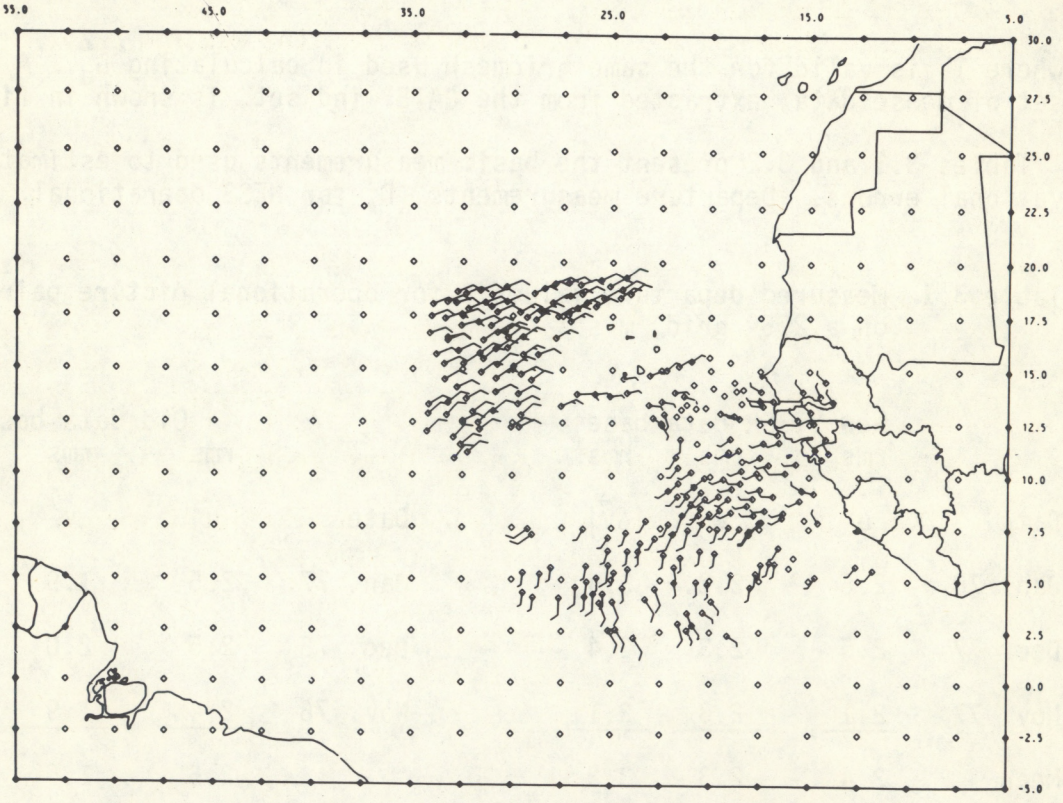

Figure 3.6--A typical set of dense cloud motion vectors from the GATE wind set, 1500 GMT, September 3, 1974.

An estimate of E_d for the GATE winds may be made from eq. (3.6) and the values in table 3.2 if we assume that a grid mesh of 1^o is sufficiently small to permit T to be neglected and yet large enough so there are sufficient observations to permit $\bar{E}^2$ to be neglected also. On basis of those assumptions, we may say that the GATE Wind sets display random rms errors

of 1.5 m s^{-1} for u and v components and an rms vector magnitude error of 2.1 m s^{-1}.

To obtain similar estimates for NESS vectors, we must next evaluate T from eq. (3.8) for the NESS grid mesh size of 2.5°. In that equation the first term, D_d^2, is evaluated from estimates for the 2.5° grid mesh in table 3.2; the second term $*D_d^2$ is derived from the 1° grid mesh and is given in the previous paragraph. Thus the rms values (T) for u, v and the absolute magnitude of the vector difference are 1.17, 0.56, and 1.36 m s^{-1} respectively.

Eq. (3.5) is now used for estimating the random error for NESS vectors, using values of T above and the values of D from table 3.1. Unfortunately, with the information available, there is no independent means for estimating $\overline{E}^2$. This precludes the calculation of a unique value for E. We may, however, place valid limits on $\overline{E}^2$ as follows. For a very large sample the lower value of $\overline{E}^2$ should be zero. Since $\overline{E}^2$ and E^2 are both functions of random errors e, drawn from the same population, the maximum value of $\overline{E}^2$ is E^2. That is,

$$0 \leq \overline{E}^2 \leq E^2 . \qquad (3.9)$$

To obtain the range of values for E we insert into eq. (3.5) estimates of T mentioned above and values of D from table 3.1. A series of guesses of E is then inserted to calculate $\overline{E}^2$. The guesses that yield values satisfying eq. (3.9) are valid solutions. The maximum and minimum of these solutions are listed in table 3.3. This shows that the self-comparison method estimates "system noise" in picture pair vectors to be in the range from 2 to 3 m s^{-1} with a probable value of 2.5 m s^{-1} rms vector magnitude.

Table 3.3 Estimates of the random observational errors of NESS low level cloud motion vectors

New VISSR data base
rms error estimates, m s^{-1}

u		v		$\lvert\delta\vec{V}\rvert$	
Min	Max	Min	Max	Min	Max
1.5	2.0	1.6	2.2	2.2	3.0

Old data base
rms error estimates, m s^{-1}

u		v		$\lvert\delta\vec{V}\rvert$	
Min	Max	Min	Max	Min	Max
1.6	2.2	1.3	1.8	2.0	2.7

3.2 Errors in Low Cloud Vectors Calculated from Tracking Experiments

Experiments described in this section were devised to evaluate the accuracy of tracking clouds over water under optimal conditions and under degraded conditions in order to assess the effect of less-than-optimal condition, viz. those that simulate picture pair computations (Bristor 1975). This procedure provides an estimate of errors in the picture pair measurements and indicates the amount of accuracy lost by using low resolution imagery.

Experiments were performed with the Goddard Space Flight Center equipment known as AOIPS (Atmospheric and Oceanographic Information Processing System) (Billingsley 1976). With that system, identical cloud targets can be tracked by different techniques on a given sequence of pictures or on the same scene displayed at different resolution, in either IR or visible form. In addition, diagnostic parameters are displayed so that a uniform, high level of quality control can be maintained. These are:

1. Motions of a given target which are measured with a sequence of images are also measured between successive images. In a 4-image sequence, for example, in addition to the vector for the entire period, vectors are also calculated from image 1 to image 2, from 2 to 3, and from 3 to 4. Large dispersion marks questionable sets.

2. Where tracking is performed by correlation, the sharpness of the correlation peak is displayed, and

3. A warning appears if the correlation peak lies on the boundary of the search area.

4. After the above items appear in digital form, a cursor on the animated display is also animated and flies along with the velocity just computed. It is easy for the operator to see if the calculated displacement is indeed the motion he attempted to follow.

Vectors may be calculated on AOIPS by three methods: manually or by either of two computer (correlation) algorithms. Correlations are performed automatically after the operator has selected an initial array and the larger search array by means of a cursor controlled by a joy-stick. Either the standard linear correlation algorithm or the Euclidean Norm (SSEC Staff 1972) may be used. Under some conditions these two algorithms yield different results but for the cloud patterns used here, the vectors they produce are virtually identical. For that reason only the Euclidean Norm algorithm was used to obtain computer-derived vectors.

3.2.1. Description of the Experiments

Cloud vectors were derived from four-image sequences that displayed the tropical Atlantic for the period 11:30 to 13:00 GMT, September 15, 1974. Figure 3.7 is the 12:30 GMT visible picture from that period. Vectors for

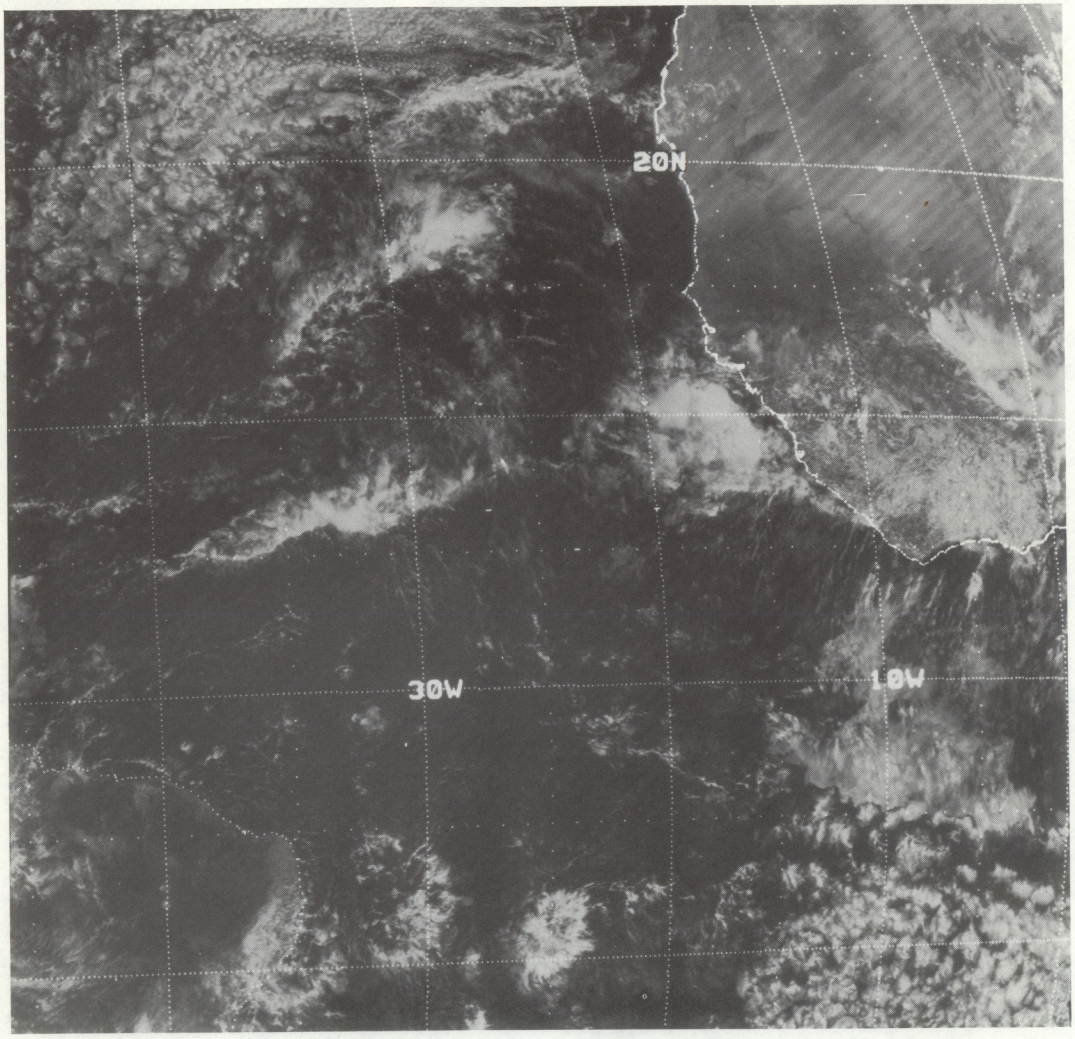

Figure 3.7--Visible picture for 12:30 GMT, September 15, 1974, showing area used in the AOIPS tracking experiment.

the three half-hour intervals were calculated as well as the motions for 90 minutes. Only low clouds of a carefully selected type were tracked--targets chosen for their high visibility on both infrared and visible pictures and for their stable behavior. This selection, together with precise registration with high resolution imagery and the moderately long tracking interval, afforded optimal conditions. Accuracy was maximized.

After tracking a large number of targets by different methods, various vector subtractions were made and summarized in table 3.4. Each vector set is described at the bottom of that table and the column headings indicate the subtractions. A right-handed coordinate system, illustrated in figure 3.8, was employed and four different parameters are identified on that figure.

Table 3.4 Differences between low cloud tracks derived by various methods over a 90-minute interval, degrees, m s^{-1}

	Visible			Infrared	
	(A-B)	(A-C)	(A-D)	(A-E)	(A-F)
DIR alg. mean	$\pm 0^{o}$	-5^{o}	$\pm 0^{o}$	-1^{o}	$\pm 0^{o}$
abs. mean	6	12	8	11	12
DIFF rms	9	19	10	16	16
STRM alg. mean	.26	-.17	.66	-.10	.18
abs. mean	.93	1.37	1.20	1.35	1.31
DIFF rms	1.19	1.74	1.84	1.72	1.72
NML alg. mean	± 0	-.08	± 0	-.02	± 0
abs. mean	.10	.21	.14	.18	.21
DIFF rms	.15	.30	.18	.26	.27
VCTR MAGN mean	.95	1.41	1.25	1.41	1.36
DIFF rms	1.20	1.76	1.86	1.74	1.74
Number (N)	34	36	32	35	32

Each column summarizes the vector-by-vector subtraction of cloud motions derived for the following sets:

A : Manual tracking on 1 km visible images.
B : Computer correlation with Euclidean Norm algorithm on 1-km visible images.
C : Manual tracking on 8 km resolution visible images.
D : Computer correlation with Euclidean Norm algorithm on 8-km visible images.
E : Manual tracking on 8 km infrared images.
F : Computer correlation with Euclidean Norm algorithm on 8-km infrared images.

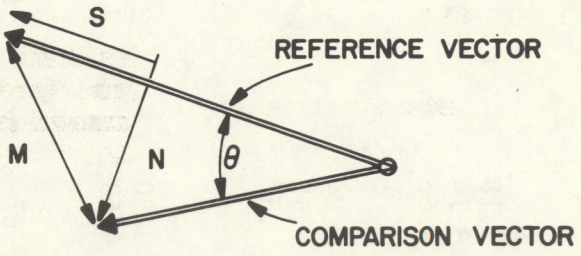

θ = Directional difference (DIR DIFF)
S = Difference along streamline (STRM DIFF)
N = Difference normal to streamline (NML DIFF)
M = Magnitude of vector difference (VCTR MAGN DIFF)

Figure 3.8--Coordinate system used with the AOIPS tracking experiment to measure along-track and cross-track and directional differences.

3.2.2 Estimates of Error under Optimal Conditions

Column (A-B) of table 3.4 provides an estimate of the vector magnitude rms error of the most accurate motion measurements. The other columns are used to deduce the additional errors introduced by resolution reduction.

That the first column of table 3.4 represents the greatest accuracy is attested to by the small differences and by reference to table 3.5. The latter shows different levels of noise caused by the irregularity of motion from one 30-minute displacement to the next. Principal causes of this zig-zag motion, in order of decreasing importance are:

- residual error of registration (image navigation)
- dispersion created by the uncertainty of locating the precise outline, or other trackable feature, on successive pictures, and
- the granularity of measurements due to pixel (picture element) size.

The real acceleration of targets in this experiment appeared to be small and is neglected.

In the absence of systematic differences, the set with the least noise of this type must be the most accurate. Table 3.4 shows the lack of systematic difference while table 3.5 indicates that high resolution vector sets are the most accurate (least noisy). This confirms the subjective impression gained during this experiment by inspection of the "flying cursor" used for quality control.

Table 3.5 Differences between cloud motions measured over three successive 30-minute intervals, degrees, m s^{-1}

		High resolution		Low resolution			
		Manual (A)	Euc.Norm (B)	Manual (C)	Euc.Norm (D)	Manual (E)	Euc.Norm (F)
DIR	alg. mean	$\pm 0^{o}$	$\pm 0^{o}$	1^{o}	-1^{o}	3^{o}	-1^{o}
	abs. mean	12	9	23	11	33	22
DIFF	rms	15	14	29	15	42	30
STR	alg. mean	-.25	-.40	-.07	-.43	1.18	.84
	abs. mean	1.47	1.15	2.80	1.55	3.74	3.10
DIFF	rms	1.86	1.45	3.51	2.01	4.65	4.25
NML	alg. mean	± 0	.01	.03	-.01	.04	-.01
	abs. mean	.21	.16	.37	.19	.49	.35
DIFF	rms	.26	.23	.44	.26	.57	.45
VCTR MAGN	mean	1.50	1.18	2.86	1.61	3.80	3.15
DIFF	rms	1.88	1.47	3.54	2.01	4.68	4.27
Number (N)		72	62	65	63	67	67

One further detail should be examined before estimating error, viz. the effect of interpolating between integral pixels in set B (computer tracked) and no interpolation in set A (manually tracked). In the manual method, target location can be no more precise then ± 0.5 pixel and it is estimated in practice to be $\pm$ one pixel, or a range of 2 km. Using the approximation that the range represents about $\pm$ 3 standard deviations, we estimate that the rms error introduced by lack of interpolation is 1/3 km. Over a 90-minute interval this amounts to but 0.06 m s^{-1}--insignificant relative to the errors listed in table 3.4. It can be neglected.

We now assume that the errors in different methods of cloud tracking are random and uncorrelated. Consequently the differences in the first column table 3.4 are comprised of the sum of two equal "method" errors. The vector magnitude of the absolute error of each method is therefore

$$\sqrt{1.20^2/2} = 0.85 \text{ m s}^{-1} \text{ rms.}$$

Table 3.4 also shows that errors are mostly along the direction of flow so that streamline differences (STR DIFF) are quite similar to vector magnitude differences. While the algebraic mean of "STRM" differences are positive, the bias is insignificant compared to the rms.

In summary, the foregoing analysis indicates that the error inherent in tracking clouds under the most favorable conditions amounts to 0.85 m s^{-1} rms, which is made up mostly of speed dispersion and has no significant bias. From this base we can now assess the additional error caused by degraded resolution.

3.2.3 Error Incurred by Reduced Resolution

If all errors are random and uncorrelated,

$$\sigma_r^2 = \sigma_t^2 - \sigma_o^2$$

where σ_t = rms values in table 3.4, columns 2 through 5,

σ_o = rms of cloud tracked under optimal conditions = 0.85 m s^{-1}

σ_r = rms due to resolution reduction from 1 km to 8 km.

Using the above equation and the values from table 3.4 gives,

(A-C) : $(1.76^2-.85^2)^{1/2} = 1.54$ m s^{-1}

(A-D) : $(1.86^2-.85^2)^{1/2} = 1.65$ "

(A-E) : $(1.74^2-.85^2)^{1/2} = 1.52$ "

(A-F) : $(1.74^2-.85^2)^{1/2} = 1.52$ "

In view of the sample size a better value derived from combining them to yield:

$$\sigma_r = 1.56 \text{ m s}^{-1} \text{ rms.}$$

As with the high resolution differences, we note that errors are chiefly in direction of the flow and that bias is not significantly different from zero.

While table 3.4 appears to indicate that visible 8-km imagery has no advantage over infrared imagery (compare column 2 to 4 and column 3 to 5), note that this is the consequence of target selection. All clouds selected for this experiment were easily distinguishable from their background in both visible and infrared pictures. This is not always the case. In some situations cloud elements are not resolved on infrared pictures. Then the field is uniform and no trackable features appear. By contrast the visible image, even when reduced to 8-km resolution, displays trackable features and brightness variance exceeding by two orders of magnitude the variance of infrared temperatures.

3.2.4 Errors Added by Decreased Time Interval

Errors estimated in the foregoing subsections pertain to cloud motions for 90 minutes. They are not representative of the NESS picture pair vectors which are derived from a single 30-minute interval. Larger errors are expected because of the following:

Residual registration error is an important source of noise in cloud tracks. It is particularly damaging to the measurement of slowly moving targets. Consider a cloud speed of 5 m s^{-1} which corresponds to a displacement of 9 km in 30 minutes. A registration error of one pixel produces a vector error of 11% with high resolution sequences and 89% with 8-km resolution. While the mean registration error averaged over many sequences is less than one pixel, the accuracy of measuring displacement depends upon the accuracy of registering each sequence. These considerations lead us to anticipate error from this source which is inversely proportional to the distance (hence to the time) over which clouds are tracked. Table 3.6 supports this contention.

Table 3.6 lists the rms "noise" compared in the same way as for table 3.5 but pertains only to computer-tracked vectors. Time differences for 30- and 60-minute intervals are shown to illustrate the increase of variance with decreasing time. The first two columns are most representative of this effect because sequences from which these were calculated were registered with 1 km data. Variance of vector magnitudes in the first column is larger by a factor of 1.92 than variance in the second column (Ratio of the rms values squared). This is in reasonable agreement with expected factor of 2.

Table 3.6 Increase of "noise" in computer-tracked vectors associated with halving the time interval, degrees, m s^{-1}

Time Interval		Visible				Infrared	
		High resolution		Low resolution			
		30 min.	60 min.	30 min.	60 min.	30 min.	60 min.
DIR	alg. mean	$\pm 0^{o}$	$\pm 0^{o}$	-1^{o}	$\pm 0^{o}$	-1^{o}	-1^{o}
	abs. mean	9	4	11	4	22	11
DIFF	rms	14	6	15	5	30	18
STR	alg. mean	-.40	-.57	-.43	-.37	.84	.11
	abs. mean	1.15	.82	1.55	.77	3.10	1.58
DIFF	rms	1.45	1.06	2.01	1.07	4.25	2.55
NML	alg. mean	.01	± 0	-.01	-.01	-.01	-.01
	abs. mean	.16	.07	.19	.09	.35	.18
DIFF	rms	.23	.10	.26	.11	.45	.26
VCTR MAGN	mean	1.18	.84	1.61	.80	3.15	1.61
DIFF	rms	1.47	1.06	2.01	1.08	4.27	2.57
Number	(N)	62	38	63	36	67	42

Larger increases with decreasing time shown in the other columns are due in part to registration error. That is, registration error of image 1 relative to 3 is independent of the registration error of image 2 to 4. Differences between those errors would add to the differences due to the increased time.

The increase of error with decreasing time can now be used to estimate the error for 30-minute interval vectors that have been measured with 8-km resolution imagery, i.e., conditions that simulate the NESS picture pair calculation. The absolute error for 8-km data was found to be 1.56 m s^{-1} rms when derived from 90-minute intervals. Reducing the tracking interval by a factor of 3 is expected to increase the rms error by:

$$\sqrt{3} \times 1.56 = 2.7 \text{ m s}^{-1}.$$

To summarize these experiments, we note that:

- With optimal target selection and for 90-minute intervals, on high resolution imagery, the error of tracking clouds may be as little as 0.85 m s^{-1} rms.
- Loss of accuracy caused by reducing image resolution from 1 km to 8 km, approximately doubles the rms error, apparently due to greater granularity of the measurements and blurring of the cloud features.
- The estimated error for picture pair vectors which is deduced by these experimental means is comparable with the estimates reported in section 3.1 and summarized in table 3.3.

3.3 Errors in Low Cloud Vectors Calculated from Simultaneous Measurements

GOES East at 75°W and GOES West at 135°W, identical spacecraft operated by NESS, view a common area in the western Gulf of Mexico and the Eastern Pacific. Cloud motions are measured from both satellites. While the procedures for deriving cloud motions are identical, the calculations are independent. That is, data ingest, movie loop production, picture pair and movie loop measurements are independent of each other and independent from one data set (time period) to another. Differences between simultaneous colocated cloud vectors provide a measure of system noise which is comprised of the sum of error in tracking cloud targets, random and bias error of registration, etc. Considerations of cloud height do not enter.

3.3.1 Data and Method of Analysis

Simultaneous vectors were analyzed for two periods, approximately a year apart, as follows:

	Number of simultaneous Vectors	
	picture pair	manual
April 12-May 12, 1977	866	259
July 1978	776	65

Colocated vectors were resolved into u and v components and subtracted. Individual vector magnitude differences were then calculated. These differences were assembled for each data set in 1977 in order to study the effect of registration bias, etc. (Hubert 1977). The 1978 data were summarized only for the entire period. Table 3.7 shows summaries for both years.

Table 3.7 Vector magnitude differences between co-located simultaneous cloud vectors, m s^{-1}

Data	N	Mean speed	Mean diff.	Diff rms	$(rms^2/2)^{1/2}$
Picture pair vectors					
Spring 1977	866	9.3	3.4	4.3	3.0
July 1978	776	9.5	3.8	4.5	3.2
wgtd mean		9.4	3.6	4.4	3.1
Manual vectors					
Spring 1977	259	30.4	4.2	4.7	3.3
July 1978	65	15.6	5.4	6.6	4.7
wgtd mean		27.4	4.4	5.1	3.6

3.3.2 Results

Differences shown in table 3.7 include errors both random and systematic. Previous analysis of the 1977 data (Hubert 1977) showed there was insignificant bias for the period as a whole, but that biases did exist in individual data sets. The contrast between the 1977 and 1978 manual vectors might be due to excessive bias in the latter, as suggested later, but we have no ready means of checking that speculation.

As in the preceding sections, we can assume that these differences result from two equally noisy measurements and divide the variance equally. This is shown in the last column of table 3.7 and represents the rms system noise attributed to each satellite system.

In summary, system noise evaluated from simultaneous measurements is:

Picture pair 3.0 to 3.1 m s^{-1} rms vector magnitude

Manual vectors 3.3 to 4.7 m s^{-1} rms vector magnitude.

In view of the small sample size, the maximum of 4.7 m s^{-1} for manual vectors may be due to excessive registration error. Since this systematic error depends so critically upon the care and skill of the photo technician who registers the movie loops, bias is likely to vary widely from time to time. Moreover, in mid-July 1977 a new spacecraft replaced GOES 1 at

135° west. For a time the orbital parameters were less accurately known and this could have contributed to cloud tracking errors. We might regard this large value as an upper limit rather than a typical error.

3.4 Summary of Errors in Cloud Tracking (System Noise)

Three methods have been used to estimate the vector magnitude rms error that exists in NESS operational picture pair cloud motions, with the following results:

Self-comparison	2.0 to 3.0 m s^{-1}	rms Vector Magnitude
AOIPS experiments	2.7 m s^{-1}	" "
Simultaneous measurements	3.1 m s^{-1}	" "

The first two are indirect and the results depend to various degrees on assumptions that variability is random and independent. The largest error estimate, from simultaneous measurements, is sensitive to registration error. Each data set (time period) contains some systematic error from this cause and thereby increases the error attributed here to "random" error. This may be responsible for this largest estimate.

The GATE Wind Sets provided data density that yielded a more precise assessment of the rms error in the self-comparison analysis and it was shown to be about 2.0 m s^{-1}. The relatively sparse picture pair data could not be analyzed with this precision; rather, the rms errors are based on estimates of upper and lower limits. Therefore it is not possible, on basis of the available data, to conclude whether the apparent advantage of the GATE Wind set (table 3.2) over the picture pair data (table 3.3), is real.

Simultaneous measurements provided a measure of the noise in manual cloud vectors that ranged up to 4.7 m s^{-1} rms vector error. An earlier analysis of these data (Hubert 1977) suggested that this larger figure may be due to a bias arising from registration error. While each movie loop registration can introduce a bias to each data set, it is not systematic from one sequence to the next. For that reason this type of bias is legitimately included here in the estimate of rms error.

While these error estimates vary, the important result is that the basic system noise is about 2.5 m s^{-1} rms vector error for picture pair vectors and perhaps 4 m s^{-1} for manual vectors.

This study of system noise suggests that the wind-derivation procedure could be improved. The AOIPS experiments showed that the rms error of low level clouds could be halved by using high resolution pictures. Therefore visible high resolution data should be used whenever possible.[4] Similar

[4]The advantage noted here concerns only registration. But sometimes the most effective targets, discernible on high resolution visible pictures, cannot be seen on infrared pictures. In such situations, the advantage of the former is even greater.

study was not performed for upper level clouds. Systematic error from this source could be virtually eliminated by computer-registration and electronic display of sequences.

4. SUMMARY AND CONCLUSIONS

Comparison of satellite winds with rawinsonde observations, together with some reasonable assumptions, yield estimates of error in measuring wind from satellites by the NESS operational system:

	rmse
900-mb wind measured with picture pairs	4.7 m s^{-1}
Upper level winds at variable heights above 700 mb.	8.5 m s^{-1}

These errors in measuring wind are comprised of a highly variable component related to atmospheric variables such as shear, and a component we call system noise which depends on the accuracy with which clouds can be tracked with satellite imagery.

Three independent methods have been used to evaluate system noise. We find about 2.5 m s^{-1} rms vector magnitude for picture pair vectors and about 4 m s^{-1} rms for manual vectors measured with movie loops.

Having the total wind error and one component (system noise) we cannot resist subtracting them to find the component due to atmosphere-related errors. That is,

$$(4.7^2-2.5^2)^{1/2} = 4.0 \text{ m s}^{-1} \text{ for low cloud winds and}$$

$$(8.5^2-4.0^2)^{1/2} = 7.5 \text{ m s}^{-1} \text{ for upper cloud winds.}$$

But these figures must be viewed with caution. Their validity depends upon the components being independent random variables. This may not be the case. It is easy to conceive of situations where both cloud tracking and height assignment errors vary together. If these are positively correlated, another subtractive term will appear under the root bracket. This exercise, at best, suggests an upper limit of errors caused by atmospheric effects. Whatever their magnitude, it appears that a significant share of the atmosphere-induced errors arises from improper height assignment. Next in importance is the effect of nonadvective cloud propagation such as gravity waves. Every data set includes a few cloud vectors that do not correspond to winds at any level. Although the latter are few in number, they are responsible for many of the largest vector errors.

The AOIPS experiments and an earlier analysis of simultaneous vectors show that the NESS winds could be improved by reducing the basic system noise by means of:

- Using high resolution, visible, imagery whenever possible and,
- Replacing photographic movie loops which are registered manually with electronically-displayed animation of sequences that have been registered by computer.

These improvements can be realized with an interactive system.

Finally, it must be emphasized that reduction of error is by no means the only or the most effective way of improving these data. Accuracy is essential, of course, but the gold assay of this meteorological ore will become high only when winds are measured in meteorologically active regions. Routine picture pair procedures avoid such active regions. The result is very low grade ore. Picture pair machinery is capable of mining only low grade ore. The nuggets must be extracted with an interactive system operating on high resolution satellite imagery.

ACKNOWLEDGEMENT

The experiments performed on the AOIPS equipment at the Goddard Space Flight Center were made possible by the generous support of many people in the GSFC Laboratory for Atmospheric Science. They provided necessary training and scheduled ample time on the system for our work.

5. REFERENCES

Arnold, A., "Representative winds aloft," Bulletin AMS, Vol. 37, No. 1, Jan. 1956, pp. 27-30.

Bauer, Kenneth G., "A comparison of cloud motion winds with coinciding radiosonde winds," Monthly Weather Review, Vol. 104, No. 7, July 1976, pp. 922-931.

Billingsley, J., "Interactive image processing for meteorological applications at NASA/Goddard Space Flight Center," Proceedings of the Seventh Conference on Aerospace and Aeronautical Meteorology and Symposium of Remote Sensing from Satellites, Melbourne, Fla., Nov. 16-19, 1976, pp. 16-19.

Bristor, C. L., Editor, "Central processing and analysis of geostationary satellite data," NOAA Technical Memorandum, NESS 64, Washington, D. C., Mar. 1975, 155 pp.

Chatters, Gary C., and Norton, Carl C., "Winds sets for GATE from SMS image cloud tracking," NOAA Contract 6-35311 Report, June 1977 by Space Science and Engineering Center, Madison, Wisconsin, June 1977, 8 pp. and two appendices.

Gabriel, J. E., and Bellucci, R., "Time variation of winds aloft," Journal of Meteorology, Vol. 8, No. 6, Dec. 1951, pp. 422-423.

Hasler, A. F., Shenk, W., and Skillman, W., "Wind estimates from cloud motions: Phase 1 of an in situ aircraft verification experiment," Journal of Applied Meteorology, Vol. 15, No. 1, Jan. 1976, pp. 10-15.

_____, _____, _____, "Wind estimates from cloud motions: Results from Phases I, II and III of an in situ aircraft verification experiment," Journal of Applied Meteorology, Vol. 16, No. 8, Aug. 1977, pp. 812-815.

Hubert, L. F., "The relation between cloud pattern motion and wind shear," Monthly Weather Review, Vol. 104, No. 9, Sept. 1976, pp. 1167-1171.

_____, "Comparison of simultaneous, co-located cloud motions measured from satellites, An unpublished internal report National Environmental Satellite Service, Washington, D. C., June 1977, 16 pp.

_____ and Whitney, L. F., Jr., "Compatibility of low-cloud vectors and rawins for synoptic scale analysis," NOAA Technical Report, NESS 70, Oct. 1974, 26 pp.

Martin, D. W., Chatters, Gary C., and Suchman, David, "GATE area wind sets from SMS Images," NASA Contract NAS 5-23296 Report, October 1975, Space Science and Engineering Center, Madison, Wisconsin, Oct. 1975, 111 pp.

Staff, SSEC, "McIDAS, An interim report on the development of the man-computer interactive data access system," An unpublished report by the Space Science and Engineering Center, Madison, Wisconsin, Nov. 1972, 29 pp.

(Continued from inside front cover)

NOAA Technical Reports

NESS 57 Table of Scattering Function of Infrared Radiation for Water Clouds. Giichi Yamamoto, Masayuki Tanaka, and Shoji Asano, April 1971, 8 pp. plus tables. (COM-71-50312)

NESS 58 The Airborne ITPR Brassboard Experiment. W. L. Smith, D. T. Hilleary, E. C. Baldwin, W. Jacob, H. Jacobowitz, G. Nelson, S. Soules, and D. Q. Wark, March 1972, 74 pp. (COM-72-10557)

NESS 59 Temperature Sounding From Satellites. S. Fritz, D. Q. Wark, H. E. Fleming, W. L. Smith, H. Jacobowitz, D. T. Hilleary, and J. C. Alishouse, July 1972, 49 pp. (COM-72-50963)

NESS 60 Satellite Measurements of Aerosol Backscattered Radiation From the Nimbus F Earth Radiation Budget Experiment. H. Jacobowitz, W. L. Smith, and A. J. Drummond, August 1972, 9 pp. (COM-72-51031)

NESS 61 The Measurement of Atmospheric Transmittance From Sun and Sky With an Infrared Vertical Sounder. W. L. Smith and H. B. Howell, September 1972, 16 pp. (COM-73-50020)

NESS 62 Proposed Calibration Target for the Visible Channel of a Satellite Radiometer. K. L. Coulson and H. Jacobowitz, October 1972, 27 pp. (COM-73-10143)

NESS 63 Verification of Operational SIRS B Temperature Retrievals. Harold J. Brodrick and Christopher M. Hayden, December 1972, 26 pp. (COM-73-50279)

NESS 64 Radiometric Techniques for Observing the Atmosphere From Aircraft. William L. Smith and Warren J. Jacob, January 1973, 12 pp. (COM-73-50376)

NESS 65 Satellite Infrared Soundings From NOAA Spacecraft. L. M. McMillin, D. Q. Wark, J.M. Siomkajlo, P. G. Abel, A. Werbowetzki, L. A. Lauritson, J. A. Pritchard, D. S. Crosby, H. M. Woolf, R. C. Luebbe, M. P. Weinreb, H. E. Fleming, F. E. Bittner, and C. M. Hayden, September 1973, 112 pp. (COM-73-50936/6AS)

NESS 66 Effects of Aerosols on the Determination of the Temperature of the Earth's Surface From Radiance Measurements at 11.2 m. H. Jacobowitz and K. L. Coulson, September 1973, 18 pp. (COM-74-50013)

NESS 67 Vertical Resolution of Temperature Profiles for High Resolution Infrared Radiation Sounder (HIRS). Y. M. Chen, H. M. Woolf, and W. L. Smith, January 1974, 14 pp. (COM-74-50230)

NESS 68 Dependence of Antenna Temperature on the Polarization of Emitted Radiation for a Scanning Microwave Radiometer. Norman C. Grody, January 1974, 11 pp. (COM-74-50431/AS)

NESS 69 An Evaluation of May 1971 Satellite-Derived Sea Surface Temperatures for the Southern Hemisphere. P. Krishna Rao, April 1974, 13 pp. (COM-74-50643/AS)

NESS 70 Compatibility of Low-Cloud Vectors and Rawins for Synoptic Scale Analysis. L. F. Hubert and L. F. Whitney, Jr., October 1974, 26 pp. (COM-75-50065/AS)

NESS 71 An Intercomparison of Meteorological Parameters Derived From Radiosonde and Satellite Vertical Temperature Cross Sections. W. L. Smith and H. M. Woolf, November 1974, 13 pp. (COM-75-10432)

NESS 72 An Intercomparison of Radiosonde and Satellite-Derived Cross Sections During the AMTEX. W. C. Shen, W. L. Smith, and H. M. Woolf, February 1975, 18 pp. (COM-75-10439/AS)

NESS 73 Evaluation of a Balanced 300-mb Height Analysis as a Reference Level for Satellite-Derived soundings. Albert Thomasell, Jr., December 1975, 25 pp. (PB-253-058)

NESS 74 On the Estimation of Areal Windspeed Distribution in Tropical Cyclones With the Use of Satellite Data. Andrew Timchalk, August 1976, 41 pp. (PB-261-971)

NESS 75 Guide for Designing RF Ground Receiving Stations for TIROS-N. John R. Schneider, December 1976, 126 pp. (PB-262-931)

NESS 76 Determination of the Earth-Atmosphere Radiation Budget from NOAA Satellite Data. Arnold Gruber, November 1977, 31 pp. (PB-279-633)

NESS 77 Wind Analysis by Conditional Relaxation. Albert Thomasell, Jr., January 1979.

NESS 78 Geostationary Operational Environmental Satellite/Data Collection System. July 1979, 88 pp.

NOAA SCIENTIFIC AND TECHNICAL PUBLICATIONS

The National Oceanic and Atmospheric Administration was established as part of the Departme Commerce on October 3, 1970. The mission responsibilities of NOAA are to assess the socioeconomic i of natural and technological changes in the environment and to monitor and predict the state of the solid l the oceans and their living resources, the atmosphere, and the space environment of the Earth.

The major components of NOAA regularly produce various types of scientific and technical inf tion in the following kinds of publications:

PROFESSIONAL PAPERS — Important definitive research results, major techniques, and special investigations.

CONTRACT AND GRANT REPORTS — Reports prepared by contractors or grantees under NOAA sponsorship.

ATLAS — Presentation of analyzed data generally in the form of maps showing distribution of rainfall, chemical and physical conditions of oceans and atmosphere, distribution of fishes and marine mammals, ionospheric conditions, etc.

TECHNICAL SERVICE PUBLICATIONS — Reports containing data, observations, instructions, etc. A partial listing includes data serials; prediction and outlook periodicals; technical manuals, training papers, planning reports, and information serials; and miscellaneous technical publications.

TECHNICAL REPORTS — Journal quality with extensive details, mathematical developments, or data listings.

TECHNICAL MEMORANDUMS — Reports of preliminary, partial, or negative research or technology results, interim instructions, and the like.

Information on availability of NOAA publications can be obtained from:

ENVIRONMENTAL SCIENCE INFORMATION CENTER (D822)
ENVIRONMENTAL DATA AND INFORMATION SERVICE
NATIONAL OCEANIC AND ATMOSPHERIC ADMINISTRATION
U.S. DEPARTMENT OF COMMERCE

6009 Executive Boulevard
Rockville, MD 20852

NOAA--S/T 79-152